The singlet–triplet splitting in these complexes, measured from the fluorescence and phosphorescence maxima at 77 K, is 3000 (±200) cm^{-1}, a value that is slightly less than the 3500-cm^{-1} splitting observed in Rh(I) monomers with chelating diphosphine ligands.[16,23] The Stokes shift, measured between the room-temperature absorption and fluorescence maxima, is 3600 (±100) cm^{-1}, a value approximately the same as that found from the triplet absorption and phosphorescence maxima of Rh(I) monomers.[16,23]

The phosphorescence lifetime versus temperature results indicate that emission from the higher level is partially allowed whereas emission from the lower level is forbidden. The decrease in emission intensity that occurs as the temperature is lowered suggests that the difference in the radiative rates of the levels is considerably greater than that indicated by the measured lifetimes. This is identical with the situation observed for the Rh(I) and Ir(I) monomers[15,16] and also for $[Pt_2(pop)_4]^{4-}$.[14] In consonance with this previous work we assign the phosphorescence manifold to a spin–orbit-split $^3B_{1u}$ term in D_{2h}. The accidentally degenerate higher level is assigned to B_{2u} and B_{3u} components (both dipole allowed) and the lower level to the A_u (dipole forbidden) state. Within the precision of our procedures, we find no evidence for splitting of the higher levels. The absence of any temperature effect (4.2–77 K) on the intensity of the shoulder relative to the main phosphorescence band in $[Rh_2(n\text{-}BuNC)_4(dam)_2]^{2+}$ indicates that this shoulder is vibrational and not electronic in origin.

The most unusual feature of the parameters obtained from the decay data is the small energy gap ($\Delta\epsilon$) between the spin–orbit-split levels, a factor of 5 less than the splitting obtained for Rh(I) monomers.[15,16] The inferred weak spin–orbit coupling is manifested also in the weak triplet absorption intensity (vide infra) and the observation of fluorescence; both are characteristic traits of organic molecules for which the splitting of triplet levels is on the order of tenths of wavenumbers.[24] These same manifestations of weak spin–orbit interaction have been observed in other metal dimers as well.[11,14]

Comparison of the $\Delta\epsilon$ values of the complexes yields information about the nature of the orbitals involved in the emitting manifold.[25] No significant change in $\Delta\epsilon$ was observed upon switching the bridging ligand from dpm to dam. In contrast, $\Delta\epsilon$ of Rh(I) monomers increased significantly upon substitution of arsine for phosphine ligands, presumably due to the greater spin–orbit coupling constant of arsenic ($\Delta\epsilon$ for $[Rh(Ph_2PCHCHPPh_2)_2]^+$, $[Rh(Ph_2AsCH_2CH_2PPh_2)_2]^+$, and $[Rh(Ph_2AsCHCHAsPh_2)_2]^+$ is 37.8, 44.8, and 57.6 cm^{-1}, respectively[16]). This effect corroborated the charge-transfer nature of the excited state of the Rh(I) monomers. The lack of any such dependence for these Rh(I) dimers leads us to conclude that the low-energy excited states are primarily metal centered, $\sigma^*(4d_{z^2}) \rightarrow \sigma(5p_z)$. This conclusion is in agreement with the results obtained for $[Rh_2(bridge)_4]^{2+}$ [12] and $[Pt_2(pop)_4]^{4-}$ in which a vibration superimposed on low-temperature triplet absorption[12,14] and phosphorescence[14] spectra could be identified as a metal–metal stretch.

Previous workers[1,3-5] have assigned the low-energy absorptions of Rh(I) dpm and dam bridged dimers to metal-to-ligand charge-transfer transitions. These assignments were, in part, based on the "shift" of the ~25 000-cm^{-1} band observed in Rh(I) monomers to much lower energy in the dimers.[1] The band present in monomers had been assigned earlier to a charge-transfer transition.[23] In light of the new metal-centered assignment of the dimer absorptions, the lack of an absorption band at ~25 000 cm^{-1} in the dimers indicates considerable $5p_z$ orbital character in the acceptor orbital of Rh(I) monomers.

Application of the Strickler–Berg formula[26] to the intense low-energy absorption bands of these dimers leads to predicted fluorescence radiative lifetimes within the range 15–35 ns. From the phosphorescence lifetimes, application of the formula predicts an upper limit of ~150 M^{-1} cm^{-1} for the extinction coefficients of the triplet absorptions.

Acknowledgment. This research has been supported by Air Force Office of Scientific Research Grant No. AFOSR-80-0038 and National Science Foundation Grant No. DMR-78-1008. We thank Matthey-Bishop Inc. for a generous loan of rhodium trichloride.

Registry No. $[Rh_2(t\text{-}BuNC)_4(dpm)_2](PF_6)_2$, 80533-10-4; $[Rh_2(n\text{-}BuNC)_4(dpm)_2](BPh_4)_2$, 80533-12-6; $[Rh_2(PhNC)_4(dpm)_2](PF_6)_2$, 80533-14-8; $[Rh_2(n\text{-}BuNC)_4(dam)_2](BPh_4)_2$, 80533-16-0.

(23) Geoffroy, G. L.; Wrighton, M. S.; Hammond, G. S.; Gray, H. B. *J. Am. Chem. Soc.* **1974**, *96*, 3105.
(24) El-Sayed, M. A. *Acc. Chem. Res.* **1971**, *4*, 23.
(25) Although we did not directly observe emission from the lower level in these complexes, indicated by a leveling off of the lifetime curve at low temperature, our confidence in the fit values was increased by checking the fit values of truncated data sets from Rh(I) and Ir(I) monomers in which the lower level lifetime was observed.[15] Truncation of the data sets down to a point at which the lifetime was one-half that of the lifetime of the lower level in the manifold resulted in only ±5% deviations of the $\Delta\epsilon$ values.
(26) Strickler, S. J.; Berg, R. A. *J. Chem. Phys.* **1962**, *37*, 814.

Synthesis, Microwave Spectrum, Electric Dipole Moment, Molecular Structure, and Anomeric Effect in Fluoroethylene Ozonide[1]

Kurt W. Hillig II, R. P. Lattimer, and Robert L. Kuczkowski*

Contribution from the Department of Chemistry, University of Michigan, Ann Arbor, Michigan 48109. *Received August 14, 1981*

Abstract: Twelve isotopic species of fluoroethylene ozonide (vinyl fluoride ozonide or 3-fluoro-1,2,4-trioxolane) were synthesized including the parent and all eight possible singly substituted D, ^{18}O, and ^{13}C species. The ground state microwave spectra of these were assigned as well as two excited vibrational states of the parent. The isotopic syntheses were consistent with the Criegee mechanism of ozonolysis. The dipole moment of the parent was found to be 2.317 (21) D, with principal axis components $|\mu_a| = 1.456$ (7), $|\mu_b| = 1.346$ (34), $|\mu_c| = 1.199$ (13). The ring conformation is a distorted twisted half-chair with the fluorine occupying an axial site, and with a long C–F bond length of 1.375 (5) Å and short adjacent C_F–O bonds, both of 1.382 (10) Å. The structure is rationalized in terms of the anomeric effect.

The ozonolysis of alkenes in solvents has been known for over 70 years.[2] The ozonides produced in this reaction were first explained by the mechanism proposed by Criegee (Scheme I)[3,4] and revised to include stereochemical effects.[5,6] Efforts to further

0002-7863/82/1504-0988$01.25/0

Scheme I

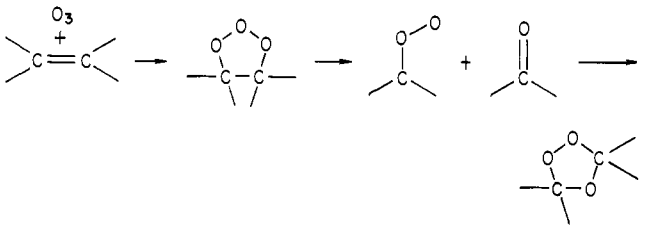

understand this process have continued along both theoretical[7-9] and experimental avenues.[10-14] More recently, attention has focussed on the ozonolysis of fluoroalkenes[15-18] which are the only members of the haloalkene class for which ozonides have been demonstrated to form in significant yield.[19-23]

One common note in many of these studies is their emphasis on the conformation and structure of the species involved. Few experimentally determined ozonide structures have been reported, with only those of ethylene ozonide (1,2,4-trioxolane; EtOz) and propylene ozonide (3-methyl-1,2,4-trioxolane; PrOz) known in detail.[5,24] The conformations of *trans*-2-butene ozonide[5] and fluoroethylene ozonide (FOz)[25] have also been reported.[26]

The axially substituted O–O twist conformation inferred for FOz in this latter study suggests that an anomeric effect[27] is operating which overrides the steric repulsion usually associated with an axial substituent. This observation motivated us to undertake the synthesis and spectral assignment of a number of isotopic species of FOz both to obtain a more detailed understanding of its structure and to give some insight into the mechanism of its formation. This was attractive because FOz is the simplest halo-ozonide and its structure is a prototype for a study of the effects of halogenation on the ozonide ring.[28] It is also a novel probe of the anomeric effect in a system rather different from the halopyranoses or halomethyl-substituted species usually studied[29] and it is interesting to see if any more subtle structural effects are associated with the conformational preference of the fluorine.[30] Finally, once the microwave spectra of the various isotopic species were known, the method of isotopic tracers could easily be employed to provide information on the mechanism of formation of a halo-ozonide.

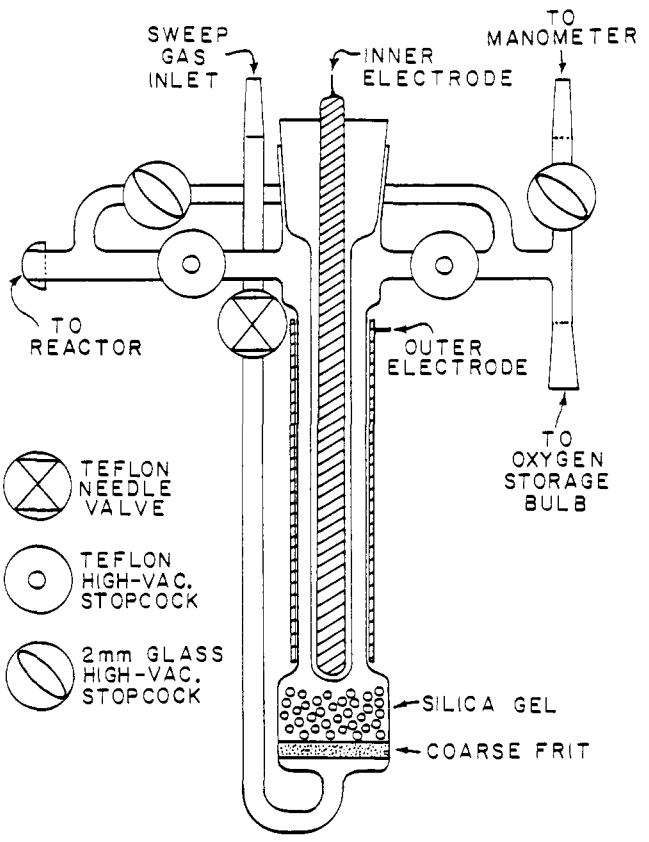

Figure 1. Ozone generator design.

Experimental Section

Synthesis. Three similar methods were used to prepare isotopically labeled species of FOz: (1) by direct reaction of vinyl fluoride (VF) with ozone; (2) by insertion of formyl fluoride (FF) in an otherwise direct reaction (see Scheme I); (3) and, indirectly as the cross-ozonide, by ozonolysis of a mixture of formaldehyde and *cis*-1,2-difluoroethylene (*cis*-DFE).

Direct reactions were run neat with 20–25 mmol VF at −126 °C. Insertion reactions were run similarly with 2–3 mmol FF added to the reaction mixture. Indirect syntheses were run in Freon 22 ($CHClF_2$; F22) at −95 °C, typically using 15 mmol of solvent, 5 mmol of *cis*-DFE, and 2.5 mmol of (monomeric) formaldehyde. All reactions and product workups were run with the use of standard high-vacuum line techniques as FOz is both water and heat sensitive. Stopcocks and ground joints

(1) Taken in part from the Ph.D. thesis of K. Hillig, University of Michigan, 1981. Portions of this work were presented as paper RF1, 34th Symposium on Molecular Spectroscopy, Ohio State University, 1979.

(2) C. Harries and K. Haeffner, *Ber.*, **41**, 3098–3102 (1908).
(3) R. Criegee and G. Wenner, *Justus Liebigs Ann. Chem.*, **564**. 9–15 (1949); R. Criegee, *ibid.*, 583, 1–36 (1953).
(4) P. S. Bailey, "Ozonation in Organic Chemistry", Vol. I, Academic Press, New York, 1978.
(5) R. P. Lattimer, R. L. Kuczkowski, and C. W. Gillies, *J. Am. Chem. Soc.*, **96**, 348–358 (1974).
(6) P. S. Bailey and T. M. Ferrell, *J. Am. Chem. Soc.*, **100**, 899–905 (1978).
(7) L. B. Harding and W. A. Goddard, *J. Am. Chem. Soc.*, **100**, 7180–7188 (1978).
(8) P. S. Nangia and S. W. Benson, *J. Am. Chem. Soc.*, **102**, 3105–3115 (1980).
(9) D. Cremer, *J. Am. Chem. Soc.*, **103**, 3619–3626, 3627–3633 (1981).
(10) G. D. Fong and R. L. Kuczkowski, *J. Am. Chem. Soc.*, **102**, 4763–4768 (1980).
(11) C. K. Kohlmiller and L. Andrews, *J. Am. Chem. Soc.*, **103**, 2578–2583 (1981).
(12) P. S. Bailey, T. M. Ferrell, A. Rustaiyan, S. Seyhan, and L. E. Unruh, *J. Am. Chem. Soc.*, **100**, 894–898 (1978).
(13) J.-S. Su and R. W. Murray, *J. Org. Chem.*, **45**, 678–684 (1980).
(14) R. I. Martinez, J. T. Herron, and R. E. Huie, *J. Am. Chem. Soc.*, **103**, 3807–3820 (1981).
(15) C. W. Gillies, *J. Am. Chem. Soc.*, **99**, 7239–7245 (1977); **97**, 1276–1287 (1975).
(16) C. W. Gillies, S. P. Sponseller, and R. L. Kuczkowski, *J. Phys. Chem.*, **83**, 1545–1549 (1979).
(17) U. Mazur, R. P. Lattimer, A. Lopata, and R. L. Kuczkowski, *J. Org. Chem.*, **44**, 3181–3185 (1979); U. Mazur and R. L. Kuczkowski, *ibid*, **44**, 3185–3188 (1979).
(18) S. P. Sponseller and C. W. Gillies, *J. Am. Chem. Soc.*, **102**, 7572–7574 (1980).
(19) K. Griesbaum and P. Hoffmann, *J. Chem. Soc.*, **98**, 2877–2881 (1976); K. Griesbaum and J. Brüggemann, *Chem. Ber.* **105**, 3638–3649 (1972).
(20) S. Vaccani, K. Kühne, A. Bauder, H. Gunthard, *Chem. Phys. Lett.*, **50**, 187–189 (1977).
(21) D. G. Williamson and R. J. Cvetanovic, *J. Am. Chem. Soc.*, **90**, 4248–4252 (1968).
(22) I. C. Hisatune, L. H. Kolopajlo, and J. Heicklen, *J. Am. Chem. Soc.*, **99**, 3704–3708 (1977); E. Sanhueza, I. C. Hisatune, and J. Heicklen, *Chem. Rev.*, **76**, 801–826 (1976).
(23) F. Gozzo and G. Camaggi, *Chim. Ind. (Milan)*, **50**, 197–199 (1968).
(24) (a) U. Mazur and R. L. Kuczkowski, *J. Mol. Spectrosc.*, **65**, 84–89 (1977); (b) R. L. Kuczkowski, C. W. Gillies, and K. L. Gallaher, *ibid.*, **60**, 361–372 (1976).
(25) R. P. Lattimer, U. Mazur, and R. L. Kuczkowski, *J. Am. Chem. Soc.*, **98**, 4012 (1976).
(26) Preliminary reports of complete structures have also recently appeared for two other ozonides: cyclopentene ozonide (6,7,8-trioxabicyclo[3.2.1]octane) by D. G. Borseth and R. L. Kuczkowski, paper RC7, 35th Symposium on Molecular Spectroscopy, Ohio State University, 1980, and private communication; 1,1-difluoroethylene ozonide by K. W. Hillig II and R. L. Kuczkowski, paper TB'5, 36th Symposium on Molecular Spectroscopy, Ohio State University, 1981 (*J. Phys. Chem.*, in press).
(27) S. Wolfe, M.-H. Whangbo, and D. J. Mitchell, *Carbohydr. Res.*, **69**, 1–26 (1979); W. A. Szarek and D. Horton, Eds., "Anomeric Effect, Origin and Consequences", ACS Symposium Series No. 87, American Chemical Society, Washington, D. C., 1979; R. U. Lemieux in "Molecular Rearrangements", P. deMayo, Ed., Interscience, New York, 1964.
(28) D. Cremer, *J. Am. Chem. Soc.*, **103**, 3633–3638 (1981).
(29) C. Romers, C. Altona, H. R. Buys, and E. Havinga, *Top. Stereochem.*, **4**, 39–97 (1969).
(30) G. A. Jeffrey, J. A. Pople, and L. Radom. *Carbohydr. Res.*, **25**, 117–131 (1972).

which came in contact with ozone were lubricated with fluorocarbon vacuum grease (Halocarbon Products Corp.).

FOz was isolated by distillation of the reaction products through −78 and −196 °C traps for 20 min. The −78 °C trap contents were used without further purification to avoid decomposition. Ozonide samples were stored under vacuum at −196 °C.

A number of explosions have occurred at various stages of the reaction/distillation process. To minimize the danger, we used no more than 1.5 mmol of ozone in any reaction, nor was more than 1 mmol of FOz collected in any sample bulb. The explosive residue in the reactor was digested for at least 24 h with 5% KI solution. All reactions were carried out inside an explosion shield fitted with extension handles for the stopcocks.

Materials. Unlabeled ozone was produced as 0.10–0.12 mmol/min O_3 in O_2 by a Welsbach T-408 ozone generator. The oxygen feed (extra dry grade) and exit streams were both dried by being passed through −78 °C traps. Labeled ozone was produced with an appropriate $^{18}O_2/^{16}O_2$ mixture (>98% $^{18}O_2$ from Prochem, BioRad, or Stohler) in the static ozone generator shown in Figure 1 (for a description of its operation, see ref 31).

Deuterium labeled VF was prepared by exchange with 1 M NaOD/D_2O at 135 °C and 15 atm (initially, decreasing slowly as the VF polymerized) in a stainless steel bomb. Approximate pseudo-first-order rate constants $K_{gem} = 6.9 \times 10^{-6}$ s^{-1}, $K_{cis} = 1.6 \times 10^{-6}$ s^{-1}, and $K_{trans} = 1.3 \times 10^{-6}$ s^{-1} were determined which reproduced the observed isotopic distributions to within 5–10%.

Paraformaldehyde-d_1 (98% D) and [^{13}C]-paraformaldehyde (90% ^{13}C) were obtained from Merck, Sharpe, and Dohme and were dried for 12 h in vacuo at room temperature before use. FF and *cis*-DFE were purchased from PCR, and F22 from Linde.

All condensible gases were dried and purified by distillation through a −78 °C trap.

Isotopic Species. ***n*-FOz (FCHOOHCHO)** was synthesized by all of the above techniques at various times, using unlabeled reactants.

***gem*-d_1-FO$_z$ (FCDOOHCHO)** was made by a direct reaction using deuterated vinyl fluoride from a 32 h exchange reaction. The VF enrichment was 19% *n*-VF, 46% 1-d_1-VF, 17% *trans*-1,2-d_2-VF, 12% *cis*-1,2-d_2-VF, and 6% d_3-VF. This species has also been observed in the products of an indirect synthesis using deuterated *cis*-DFE (prepared similarly to d_n-VF, vide supra).

***cis*- and *trans*-d_1-FOz (FCHOODCHO and FCHOOHCDO)** were made by indirect reaction, adding labeled formaldehyde (80% CHDO, 20% CH_2O) in the ozonolysis of *cis*-DFE in F22 solvent.

d_3-FOz (FCDOODCDO) was prepared by direct reaction of ozone with deuterated vinyl fluoride (2% *n*-VF, 26% 1-d_1-VF, 29% *trans*-1,2-d_2-VF, 18% *cis*-1,2-d_2-VF, 25% d_3-VF).

$^{18}O_c$-FOz (FCHOOHCH^{18}O) was prepared by indirect synthesis using labeled formaldehyde (55% $CH_2{}^{18}O$, 45% $CH_2{}^{16}O$).

$^{18}O_{F'}$, $^{18}O_{H'}$, and $^{18}O_F{}^{18}O_H$-FOz (FCH^{18}OOHCHO, FCHO^{18}OHCHO, and FCH^{18}O^{18}OHCHO) were produced simultaneously by insertion of unlabeled formyl fluoride in the ozonlysis of *n*-VF with labeled ozone, prepared from a 50/50 mixture of $^{18}O_2$ and $^{16}O_2$.

$^{18}O_3$-FOz (FC^{18}O^{18}OHCH^{18}O) was prepared by the direct reaction of VF with labeled ozone (99% ^{18}O).

$^{13}C_H$-FOz (FCHOOH^{13}CHO) was made by indirect synthesis using 50% $^{13}CH_2O$ and 50% $^{12}CH_2O$.

$^{13}C_F$-FOz (F^{13}CHOOHCHO) was prepared by insertion of ^{13}C labeled formyl fluoride prepared by Dr. A. Lopata. The reactant mixture contained approximately a 3/1 mixture of H^{13}COF/H^{12}COF which was recovered from the synthesis of labeled HCOO$^{13}CH_2F$ (see ref 31). Only 1 mmol of ozone was used in this synthesis to maximize the labeled HCOF insertion yield.

Spectrometer. Deuterium enrichment of VF was analyzed using a Hewlett-Packard 8460A MRR spectrometer.[32] As FOz is extremely unstable in the gold-plated HP cell ($t_{1/2}$ < 30 s at −70 °C) the ozonide spectra were observed with a home built Stark-modulated spectrometer[33] with a 10 ft × 1 in. × 0.5 in. brass waveguide cell and klystron sources operating in the range of 8–40 GHz. Radio frequency-microwave double resonance (RFMWDR) was used to identify certain transitions of the various species.[34] With the cell maintained between −70 and −50 °C with dry ice, the decomposition half-life of FOz was typically 5–10 min. Frequency measurements with this system are accurate to ±0.05 MHz.

Table I. Assigned Microwave Transitions of *n*-FOz ($v = 0$)[a]

transition	freq, MHz	obsd − calcd
0(0,0)-1(1,1)*	9 896.65	−0.02
1(1,1)-2(1,2)*	13 284.39	0.07
1(1,0)-2(1,1)*	14 871.69	0.02
1(0,1)-2(1,2)*	16 142.08	0.08
1(1,0)-2(2,1)*	23 444.70	0.02
1(1,1)-2(2,0)*	24 382.09	0.16
1(1,0)-2(2,0)*	23 588.41	0.15
1(1,1)-2(2,1)*	24 238.31	−0.04
1(0,1)-2(1,1)*	18 523.10	0.09
2(0,2)-3(0,3)*	20 571.27	0.01
2(1,2)-3(1,3)*	19 843.56	−0.04
2(1,1)-3(1,2)*	22 208.04	−0.02
2(2,0)-3(2,1)*	21 662.63	−0.10
2(1,2)-3(0,3)*	18 363.58	−0.10
2(0,2)-3(1,3)*	22 051.24	0.06
2(1,2)-3(2,1)*	32 760.46	0.12
2(2,0)-3(3,1)*	37 328.40	−0.43
2(2,1)-3(3,0)*	37 488.78	0.19
2(0,2)-3(1,2)*	26 796.59	−0.07
2(1,2)-3(2,2)*	32 071.10	0.08
2(1,1)-3(2,1)*	30 379.39	0.07
2(2,1)-3(3,1)*	37 472.21	−0.20
2(2,0)-3(3,0)*	37 345.83	0.44
2(2,1)-3(2,2)	21 117.21	0.21
2(1,1)-3(2,2)	29 690.49	0.48
4(0,4)-5(0,5)	33 138.67	−0.38
4(1,4)-5(1,5)	32 728.69	−0.49
4(2,2)-5(2,3)	36 920.00	−0.33
4(3,2)-5(3,3)	35 540.10	0.03
4(3,1)-5(3,2)	35 863.42	−0.11
4(0,4)-5(1,5)	33 597.27	−0.35
4(2,3)-5(1,4)	30 249.97	−0.62
4(1,4)-5(0,5)	32 270.11	−0.50
4(2,2)-5(1,4)	28 342.23	−0.55
9(5,5)-9(6,4)	34 994.92	−1.49
9(5,4)-9(6,3)	34 874.82	−1.45
9(5,5)-9(6,3)	34 999.74	−1.48
9(5,4)-9(6,4)	34 869.94	−1.53

[a] Entries with an asterisk were used in the rigid rotor fit.

Spectra. The dominant features of the spectrum are low J a- and b-dipole R-branch transitions and high J b- and c-dipole Q-branch transitions. The large asymmetry splittings ($\kappa = -0.565$)[35] preclude any obvious clustering of R-branch lines or Q-branch bandheads, and in concert with the three allowed selection rules produce a crowded spectrum. The b-dipole $J'_{K_-'K_+'} \leftarrow J''_{K_-''K_+''}$ Q-branch series for $J \geq 8$, $K_- = 6 \leftarrow 5$ (and also $K_- = 7 \leftarrow 6$ for some species) was readily identified using RFMWDR, with a radio frequency field which pumped the strong a-dipole $\Delta J = 0$, $\Delta K_- = 0$, $\Delta K_+ = \pm 1$ transitions, generally in the range of 5–20 MHz. Similarly, R-branch transitions involving the 3_{30}, 3_{31}, 5_{41}, or 5_{42} levels were generally identified by this method.

Centrifugal distortion effects were small, and the largest deviation from a rigid rotor model was ca. 1.5 MHz for the $J = 9 \leftarrow 9$ transitions. These were consequently neglected in the determination of the rotational constants. However, only transitions involving $J \leq 6$ were utilized to minimize any residual errors. The assignments of the transitions are based on the observed Stark effects, intensities, and RFMWDR behavior of the lines as well as the quality of the rigid rotor fit and the self-consistency with the structure obtained (vide infra).

Table I lists a selection of the 62 assigned transitions of *n*-FOz, while the rotational constants of all of the isotopic species are given in Table II. The uncertainty in the rotational constants for all of the species is better than ±0.05 MHz. A complete list of the assigned transitions of all of the isotopic species and the two assigned vibrational satellites is available (Tables S1–S13: Supplementary Material).

Excited Vibrational States. The spectra of two singly excited vibrational states (hereafter called V_x and V_y) were assigned. The rotational constants determined for V_x were A = 6776.82, B = 3914.91, C =

(31) A. D. Lopata and R. L. Kuczkowski, *J. Am. Chem. Soc.*, **103**, 3304–3309 (1981).
(32) A. L. Larrabee and R. L. Kuczkowski, *J. Catal.*, **52**, 72–80 (1978).
(33) K. B. McAfee, Jr., R. H. Hughes, and E. B. Wilson, *Rev. Sci. Instrum.*, **20**, 821–826 (1949).
(34) F. J. Wodarczyk and E. B. Wilson, *J. Mol. Spectrosc.*, **37**, 445–463 (1971).
(35) B. S. Ray, *Z. Phys.*, **78**, 74 (1932).

Table II. Rotational Constants of Isotopically Substituted Species of FOz

species	A, MHz	B, MHz	C, MHz	no. of assigned transitions
n-FOz	6774.00	3916.34	3122.66	62
gem-d_1-FOz	6592.96	3810.84	3091.91	19
cis-d_1-FOz	6592.65	3791.38	3039.90	19
trans-d_1-FOz	6696.80	3777.62	3036.46	13
d_3-FOz	6350.81	3565.59	2932.00	17
$^{18}O_e$-FOz	6534.60	3912.96	3071.74	10
$^{18}O_H$-FOz	6640.93	3833.81	3058.64	23
$^{18}O_F$-FOz	6535.52	3899.92	3081.29	27
$^{18}O_F{}^{18}O_H$-FOz	6415.31	3816.15	3021.19	19
$^{18}O_3$-FOz	6186.07	3813.34	2970.81	17
$^{13}C_F$-FOz	6752.65	3894.33	3113.14	20
$^{13}C_H$-FOz	6743.79	3858.98	3080.28	13

Table III. The Stark Effect in FOz

transition	M	$(\Delta\nu/E^2)_{obsd}$[a]	$(\Delta\nu/E^2)_{calcd}$
$2_{12} \leftarrow 1_{01}$	0	−4.04	−4.31
$3_{12} \leftarrow 2_{11}$	1	−8.29	−8.31
$2_{11} \leftarrow 1_{01}$	1	87.36	87.25
	0	−5.19	−5.34
$3_{13} \leftarrow 2_{12}$	2	22.17	21.95
	1	5.50	5.57
$3_{03} \leftarrow 2_{02}$	2	35.74	36.09

$|\mu_a| = 1.456 \pm 0.007$ D
$|\mu_b| = 1.346 \pm 0.034$ D
$|\mu_c| = 1.199 \pm 0.013$ D
$|\mu_t| = 2.317 \pm 0.021$ D

[a] In units of MHz kV^{-2} cm^{-2}.

3121.61 MHz, and those for V_y were A = 6762. 39, B = 3918.92, C = 3125.66 MHz. These are believed to arise from excited vibrational states and not a second conformer from the similarity of these constants to those of the parent. The lack of a simple progression in the constants implies that they do not represent succesive excitations of a single vibrational mode.

A RFMWDR search of the J = 9 Q-branch region revealed five sets of satellite transitions not assignable to any abundant naturally occurring isotopic species (the ^{13}C species' spectra were too weak to be seen in an unenriched sample). It seemed reasonable to assign these to the (V_x,V_y) = (1,0), (2,0), (1,1), (0,1), and (0,2) states. Assuming a cell temperature of −50 °C and the spectrometer sensitivity as indicated above, the observed intensities of these transitions implies an energy of 200 ± 50 cm^{-1} for the states (1,0) and (0,1). These vibrational frequencies are sufficiently high to result in typical semi-rigid rotor spectra without perturbations arising from pseudorotation or ring inversion.

Dipole Moment. The second-order Stark effects for seven M components of five transitions were measured, with a static electric field from a Fluke 412B precision high voltage DC power supply. The voltage output and electrode spacing were calibrated by using the known Stark effect and dipole moment of OCS.[36] The dipole moment components were determined by the method of Golden and Wilson[37] and are given in Table III.

Structure Calculation. Since FOz has no symmetry the moments of inertia depend on 27 Cartesian coordinates. Utilizing the six equations which define the principal axis system ($\sum_i m_i x_i = 0$, $\sum_i m_i x_i y_i = 0$, etc.) and appropriate coordinate transformations these can be reduced to 21 unique internal coordinates (structural parameters). Since data are available for 12 isotopic species, a total of 42 equations can be written to determine the 27 unknown coordinates. A least-squares fit of this 27 × 42 system yields the so-called r_0 or "effective" coordinates in Table IV and the resulting structural parameters in Table V.[38] Least-squares fits to either moment of inertia equations ($I_x = \sum_i m_i(y_i^2 + z_i^2)$, etc.) or product of inertia equations ($P_{xx} = \sum_i m_i x_i^2$, etc.) gave essentially identical results. The root mean square deviation between observed and calculated moments was 0.009 amu Å^2; the largest difference was 0.014 amu Å^2 for I_a (77.328 amu Å^2) of $^{18}O_F$-FOz.

(36) J. S. Muenter, *J. Chem. Phys.*, **48**, 4544–4547 (1968).
(37) S. Golden and E. B. Wilson, *J. Chem. Phys.*, **16**, 669–685 (1948).
(38) Conversion factor AI_a = 505379.05 MHz amu Å^2.

Table IV. r_0 Coordinates of FOz (Å)[a]

atom	a	b	c
O_e	−0.1245 (46)	1.1623 (12)	0.2114 (55)
C_F	0.7036 (57)	0.0914 (109)	0.4915 (43)
O_F	−0.0832 (48)	−1.0435 (15)	0.5419 (27)
O_H	−1.0743 (14)	−0.7453 (21)	−0.4916 (33)
C_H	−1.3814 (26)	0.5849 (38)	−0.1360 (62)
F	1.6456 (27)	−0.0002 (61)	−0.5059 (15)
H_{gem}	1.2397 (27)	0.2092 (151)	1.4332 (24)
H_{eq}	−1.7935 (20)	1.0687 (34)	−1.0119 (36)
H_{ax}	−2.0503 (18)	0.6189 (61)	0.7317 (48)

[a] The uncertainties listed represent one standard deviation in the fit.

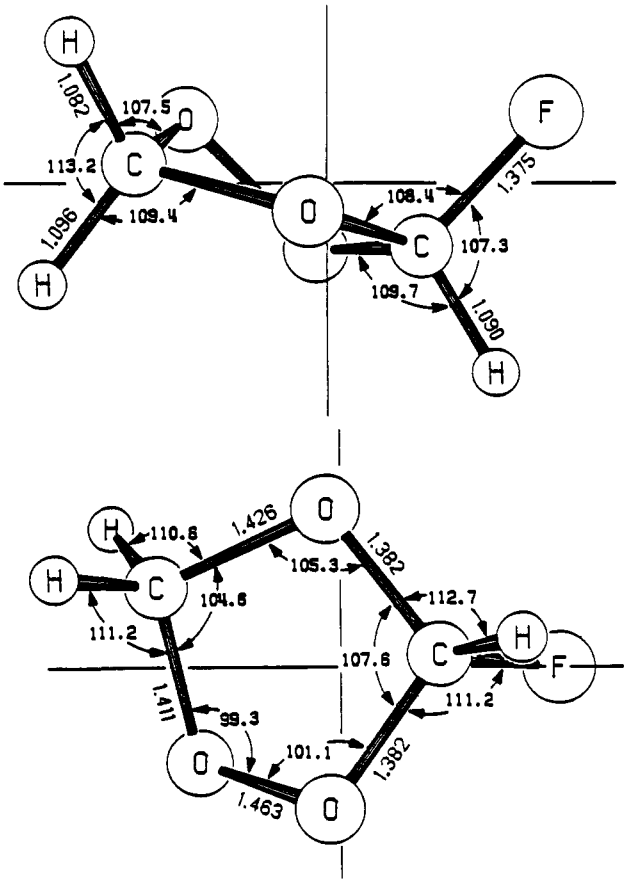

Figure 2. Principal axis projections of FOz: Top, a–c plane; bottom a–b plane.

An alternative approach is to calculate the atomic coordinates directly from the changes in moments of inertia on isotopic substitution at each site, giving the r_s or "substitution" coordinates.[39] Since isotopic substitutions of the fluorine is not possible this atom must be located by using the center-of-mass or product of inertia conditions. However, r_s structures are known in general not to fulfill these conditions[40] and the accumulation of small errors in the r_s coordinates can thus lead to a very large uncertainty in the fluorine position. Further, the substitution method is known to be unreliable for coordinates smaller than 0.1–0.15 Å[41] and FOz has five coordinates in this category. For example, the r_s a coordinate of O_F is found to be imaginary, while the b coordinate of C_F differs by 0.064 Å from its r_0 value.

Our evaluation is that the r_0 method gives the most reliable structural parameters for FOz. It utilizes all the the available data, shows excellent internal consistency, and effectively distributes the uncertainties over the entire molecular structure rather than concentrating them artificially on the fluorine or on some small coordinate. It is difficult to estimate the absolute accuracy of an r_0 structure without a detailed vibrational

(39) J. Kraitchman, *Am. J. Phys.*, **21**, 17 (1953).
(40) R. H. Schwendeman in "Critical Evaluation of Chemical and physical Structural Information", D. R. Lide and M. A. Paul, Eds., National Academy of Sciences, Washington, D.C., 1974, pp 74–115.
(41) C. C. Costain, *J. Chem. Phys.*, **29**, 864–874 (1958).

Table V. Structural Parameters of FOz[a]

bond lengths, Å		angles, deg: bond		angles, deg: dihedral	
O_e-C_F	1.382 (10)	C-O_e-C	105.3 (4)	C-O_F-O_H-C	−46.0
O_e-C_H	1.426 (5)	O-C_F-O	107.6 (4)	O-O_H-C_H-O	40.4
C_F-O_F	1.382 (10)	O-C_H-O	104.6 (2)	O-O_F-C_F-O	35.0
C_H-O_H	1.411 (5)	C-O_F-O	101.1 (3)	C-O_e-C_H-O	−20.2
O_F-O_H	1.463 (5)	C-O_H-O	99.3 (3)	C-O_e-C_F-O	10.1
C_F-F	1.375 (5)	O_e-C-F	108.4 (6)	F-C_F-O_e-C	110.3
C_F-H	1.090 (6)	O_F-C-F	111.2 (7)	F-C_F-O_F-O	−83.5
C_H-H_{eq}	1.082 (6)	O_e-C_F-H	112.7 (10)	H-C_F-O_e-C	−131.2
C_H-H_{ax}	1.096 (7)	O_F-C_F-H	109.7 (9)	H-C_F-O_F-O	158.0
		F-C-H	107.3 (5)	H_{eq}-C_H-O_H-O	158.0
		H-C-H	113.2 (4)	H_{ax}-C_H-O_H-C	−77.6
		O_e-C-H_{ax}	110.6 (4)	H_{eq}-C_H-O_e-C	−135.7
		O_H-C-H_{ax}	107.5 (5)	H_{ax}-C_H-O_e-C	99.0
		O_e-C-H_{eq}	109.4 (5)		
		O_H-C-H_{eq}	111.2 (5)		

[a] The listed uncertainties represent one standard deviation in the fit.

Table VI. Comparison of Ozonide Structures[a]

parameter	EtOz (X = H)	PrOz[b] (X = CH_3)	FOz[b] (X = F)
O_e-C_H	1.415	1.423	1.426
O_e-C_X		1.423	1.382
O_p-C_H	1.410	1.411	1.411
O_p-C_X		1.404	1.382
O_P-O_P	1.461	1.461[c]	1.463
C-O_e-C	104.6	104.6	105.3
C_H-O_P-O_P	99.2	99.2	99.3
C_X-O_P-O_P		99.7	101.1
O_e-C_H-O_P	105.7	105.7	104.6
O_e-C_X-O_P		105.6	107.6
C-O_P-O_P-C	49.4	49.2	46.0

[a] All distances are in Å, all angles are in deg. O_e = ether O; O_P = peroxy O; C_H = CH_2 carbon; C_X = CHX carbon. [b] The CH_3 is at an equatorial site. The F is at an axial site. [c] Assumed value.

analysis. It seems likely that the equilibrium structure lies within 2 standard deviations of the values listed in Table V.

All calculations were carried out with our extended version of Schwendeman's STRFIT program.[40]

Discussion

Structure. In Figure 2 the projections of FOz onto the *a*–*b* and *a*–*c* inertial planes are drawn. A comparison with the structures of EtOz and PrOz is presented in Table VI.[42]

The most interesting features of the structure are the axial position of the fluorine, rather than a sterically favored equatorial orientation, and the long C–F bond. These can be rationalized by an anomeric interaction between the fluorine and the adjacent oxygen atoms.[27]

The anomeric effect was originally expressed in terms of a conformational preference in pyranose rings with electronegative substituents but has since been generalized to include such a preference for a substituent adjacent to an oxygen in any conformationally free ring or chain structure.[43] The interaction involved is most easily visualized as a n–σ^* overlap between the C–F antibonding orbital and a π–type oxygen lone pair as shown in Figure 3. The σ,π lone pair model is preferred over a sp^3 hybrid model due both to its utility here and its better rationalization of photoelectron studies of oxygen-containing systems.[44]

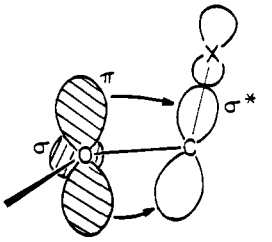

Figure 3. The anomeric orbital interaction.

This analysis is also supported by recent MO calculations on FOz which find a minimum energy structure for a conformation with an axial fluorine, very similar to our experimental structure.[28] In these calculations, Cremer has analyzed this interaction in terms of the π-donor/σ-acceptor behavior of the fluorine. The enhanced π-type overlap of the fluorine lone pairs and the ring HOMO's for an equatorial substituent are destabilizing since the HOMO's are largely antibonding. For an axial substituent this overlap is minimal and the σ-accepting interaction stabilizes the ring.

In our simplistic approach the n–σ^* interaction will be maximized if the C–F bond (or more properly the O–C–F plane) is perpendicular to the C_F–O–O plane or the C–O–C plane depending on which oxygen interaction predominates. The corresponding observed dihedral angles of 83.5° and 110.3° suggest a stronger interaction with the peroxy oxygen atom. This is plausible since the lone pair–lone pair repulsion within the O–O moiety would be expected to enhance the n–σ^* donation.

In EtOz and PrOz the O–O moiety is symmetrically disposed above and below the C–O–C plane. In FOz it is displaced ca. 5° toward the fluorine, giving an overall conformation intermediate between a pure twist (as in EtOz) and an O_H envelope. This can be seen in Figure 2 since the *a*–*c* inertial plane is almost exactly perpendicular to the C–O–C plane. This can also be interpreted as enhancing the peroxy-side interaction by bringing the X_{axial}–C–O–O angle closer to 90° (78° in EtOz, 84° in FOz). It is somewhat speculative to infer such a synergism from these angles alone since the structural parameters are constrained by the ring structure to be highly correlated and other mechanisms (vide infra) also operate to affect the overall ring geometry.

In this context the decrease in the C–O–O–C dihedral angle compared with EtOZ and PrOz is also interesting. The inductive increase in the O–C_F bond polarity would be expected to increase this angle if the dipole–dipole interaction of the O–C_H and O–C_F bonds was the major driving force determining this angle.[45] A lessened lone pair–lone pair repulsion due to the n–σ^* delocalization could explain the decrease; however, a general "flattening" of the ring is required by the decrease in length of only two of the five ring bonds. As a simple measure of this flattening, the

(42) The structure of PrOz[5] was redetermined, using the same method, but taking the O–O bond length (1.461 Å) of ref 24a rather than the original less accurate value of ref 24b. The overall effect on the structure of PrOz is small.

(43) W. F. Bailey and E. L. Eliel, *J. Am. Chem. Soc.*, **96**, 1798–1806 (1974); E. L. Eliel and C. A. Giza, *J. Org. Chem.*, **33**, 3754–3758 (1968); C. B. Anderson and D. T. Sepp, *ibid.*, **32**, 607–611 (1967); *Tetrahedron* **24**, 1707–1716 (1968).

(44) C. R. Brundle and D. W. Turner, *Proc. R. Soc. London, Ser. A.*, **307**, 27–36 (1968); M. I. Al-Joboury and D. W. Turner, *Proc. R. Soc. London, Ser. B*, **373** (1967).

(45) D. Cremer, *J. Chem. Phys.*, **70**, 1898–1910 (1979).

Table VII. Comparison of C-F Bond Lengths

compd	r_{C-F}, Å	ref
$F-CH_3$	1.385	*a*
$F-CH_2CH_3$	1.383	*b*
$F-CH_2Cl$	1.378	*c*
FOz	1.375	this work
$F-CH_2OC(O)H$	1.369	*d*
$F-CH_2COOH$ (trans)	1.365	*e*
$F-CH_2F$	1.358	*f*
$F-CH_2COF$ (trans)	1.351	*e*
$F-CHF_2$	1.326	*a*
$F-CF_3$	1.321	*g*

[a] O. R. Gilliam, H. D. Edwards, and W. Gordy, *Phys. Rev.*, 75, 1014–1016 (1949). [b] P. Nösberger, A. Bauder, and Hs. H. Gunthard, *Chem. Phys.*, 1, 418–425 (1973). [c] N. Muller, *J. Am. Chem. Soc.*, 75, 860–863 (1953). [d] Reference 31. [e] B. P. Van Eijck, P. Brandts, and J. P. M. Maas, *J. Mol. Struct.*, 44, 1–13 (1978). [f] D. R. Lide, Jr., *J. Am. Chem. Soc.*, 74, 3548–3552 (1952). [g] $r_g(0)$ value calculated from the data of M. Fink, C. W. Schmiedekamp, and D. Gregory, *J. Chem. Phys.*, 71, 5238–5242 (1979).

sum of the magnitudes of the ring dihedral angles of FOz is 151°, compared with 163° in EtOz.

The C_F–O bonds of FOz are seen to be short in comparison with the other ozonides, as is expected from simple inductive arguments for an electronegative substituent. The C–F bond, however, is some 0.03–0.04 Å longer than expected for such a model (cf. Table VII). It is apparent that donation into the C–F antibonding orbital rationalizes the long C–F bond, as has been seen in some other systems.[27,29,46] The shortening of the two C_X–O bonds is also consistent with this. Their near equivalence however does not support the inference of a somewhat stronger peroxy-side interaction implied by the dihedral angles, although geometric constraints (vide supra) may obscure this correlation.

Mechanism. Due to the low stability of FOz, it was not possible to make measurements of relative transition intensities (and thus isotopic abundance ratios) on other than a qualitative basis. Nevertheless, in each reaction it was observed that the products expected from a Criegee mechanism were present in roughly the expected proportions. For example, the synthesis of $^{18}O_F$-, $^{18}O_H$-, and $^{18}O_F{}^{18}O_H$-FOz (vide supra) resulted in transitions for the $^{18}O_3$-FOz species which were significantly weaker than those of the desired products. This suggests both that the unlabeled FF insertion proceeded as expected, and that the Criegee intermediate (H_2COO) has a lifetime under the reaction conditions (−126 °C, polar solvent) which is sufficiently long to participate significantly in out-of-cage reactions[10] rather than immediately reacting with the FF produced in the initial solvent cage.

One further test of the mechanism is the amount of ^{18}O enrichment at the peroxy (O_H) site in the ozonide resulting from the insertion of $CH_2{}^{18}O$ in the ozonolysis of *cis*-DFE. Such enrichment could only arise through a non-Criegee path. A sample of FOz prepared in this manner using 51.5 ± 1% $CH_2{}^{18}O$ and 48.5 ± 1% $CH_2{}^{16}O$ had transitions from the expected *n*-FOz and $^{18}O_e$-FOz species readily visible and of similar intensity, while those of $^{18}O_H$-FOz could not be detected. From the signal/noise of the *n*-FOz lines (ca. 20) an upper limit of 4–5% can be set for a non-Criegee peroxide enrichment pathway in the reaction. This is the first definitive aldehyde-^{18}O insertion test performed for a fluoroozonide although there have been several examples for alkyl and aryl alkenes.[47-50]

In summary, the isotopic enrichments obtained during the ozonolysis of C_2H_3F and *cis*-$C_2H_2F_2$ indicate that the mechanism of ozonide formation is similar to that of the alkyl alkenes and consistent with Scheme I.

Dipole Moment. A simple model of the molecular dipole moment considers it as the vector sum of a C–F bond moment and an ethylene ozonide group moment. For the latter we have assumed a value of 1.1 D[51] directed from the midpoint of the O–O bond to the ether oxygen, while for the former a value of 1.4 D is used. The sum of these gives component magnitudes of (1.32, 0.93, 0.93) while their difference gives (0.61, 1.12, 1.12). The former is in fair agreement with our experimental values, allowing for moderate effects of the anomeric redistribution of charge, and suggests that this choice of component directions, i.e, $(OO)^+$–O_e^- and C^+–F^-, is reasonable (although the opposite direction for both cannot be ruled out). The observed dipole moment agrees well with Cremer's calculated value of 2.35 D.[28]

Acknowledgment. This work was supported by Grants GP 38750X, CHE 76-09572, and CHE 8005471 from the National Science Foundation, Washington, D.C. We are grateful to Drs. Alexander Lopata, Ursula Mazur, and Charles Gillies for considerable advice and assistance on synthetic aspects of the research at various stages.

Registry No. *n*-FOz, 60553-18-6; *gem*-d_1-FOz, 80288-34-2; *cis*-d_1-FOz, 80288-35-3; *trans*-d_1-FOz, 80288-36-4; d_3-FOz, 80288-37-5; $^{18}O_e$-FOz, 60553-19-7; $^{18}O_H$-FOz, 80288-38-6; $^{18}O_F$-FOz, 80288-39-7; $^{18}O_F{}^{18}O_H$-FOz, 80288-40-0; $^{18}O_3$-FOz, 80288-41-1; $^{13}C_F$-FOz, 80288-42-2; $^{13}C_H$-FOz, 80288-43-3; EtOz, 289-14-5; PrOz, 38787-96-1; vinyl fluoride, 75-02-5; ozone, 10028-15-6; formyl fluoride, 1493-02-3; formaldehyde, 50-00-0; *cis*-1,2-difluoroethylene, 1630-77-9.

Supplementary Material Available: Tables S1–S12, transition frequencies for the 12 isotopic species; Table S13, frequencies for the two excited vibrational states (14 pages). Ordering information is given on any current masthead page.

(46) J. Nakagawa and M. Hayashi, *Chem. Lett.*, 349–350 (1976); G. A. Jeffrey and J. H. Yates, *J. Am. Chem. Soc.*, **101**, 820–825 (1979).

(47) C. W. Gillies, R. P. Lattimer, and R. L. Kuczkowski, *J. Am. Chem. Soc.*, **96**, 1536–1542 (1974).

(48) R. P. Lattimer and R. L. Kuczkowski, *J. Am. Chem. Soc.*, **96**, 6205–6207 (1974); K. L Gallaher and R. L. Kuczkowski, *J. Org. Chem.*, **41**, 892–893 (1976).

(49) D. P. Higley and R. W. Murray, *J. Am. Chem. Soc.*, **98**, 4526–4533 (1976).

(50) S. Fliszár and J. Carles, *J. Am. Chem. Soc.*, **91**, 2637–2643 (1969).

(51) C. W. Gillies and R. L. Kuczkowski, *J. Am. Chem. Soc.*, **94**, 6337–6343 (1972).